Computers and Geotechnics 184 (2025) 107229

Contents lists available at ScienceDirect

Computers and Geotechnics

journal homepage: www.elsevier.com/locate/compgeo

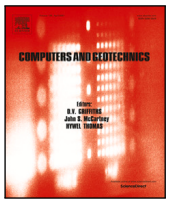

Research paper

Numerical analysis of soil arching and critical height in column-supported embankments using the Material Point Method

Wei He *, Kaibo Yang, Pingbao Yin

Changsha University of Science and Technology, 960, Wan-jia-li South Road, Changsha, 410114, Hunan, China

ARTICLE INFO

Keywords:
Column-supported embankment
Differential settlement
Soil arching effect
Material Point Method

ABSTRACT

The arching effect and critical height in column-supported embankments were studied using the Material Point Method (MPM). First, the method was validated using model and field test results. Based on these validations, additional scenarios covering various embankment heights and column spacings were analyzed using MPM. The results showed that the shear pattern evolves from a punching shear pattern for embankments lower than 0.7(s-a) to an inverted general bearing pattern for embankments higher than 1.3(s-a). These observations were further validated through numerous 3D analyses based on the soil profile of a real project. Lastly, additional case studies from China, the 3D MPM analysis results, and previously available data, were compared with existing criteria, leading to the proposal of a modified formula for the critical height of embankment to consistently reduce differential settlement to under 0.1%.

1. Introduction

Column-supported embankments are among the most effective methods for reducing settlement in roads and railways constructed over thick soft clay (Zhang et al., 2022; Pan et al., 2022). Unlike other ground improvement techniques, such as compaction and preloading, this approach does not directly enhance the soil itself. Instead, it reinforces the ground by creating a composite system where the applied loads are shared between the soil and columns (i.e. inclusions). While lower embankments generally result in reduced overall settlement, there is a significant risk of differential settlements between the columns and the center of the installed grid, as shown in Fig. 1. This risk becomes critically high when the embankment height falls below the so-called 'critical height' (Naughton, 2007), potentially compromising road serviceability. For instance, the "egg box" deformation pattern observed on pavements, as documented in the ASIRI national project report, exemplifies this problem (Simon, 2013).

The soil arching effect, which involves the transfer of pressure from a yielding mass of soil onto adjoining stationary parts (Terzaghi, 1943), plays a crucial role in investigating the critical height of column-supported embankments. This phenomenon was first studied by Terzaghi through a trapdoor experiment, which revealed that at elevations greater than approximately 2.5 times the clear spacing of the yielding strip, the state of stress in the sand remained unaffected. Although Terzaghi's research did not specifically target column-supported embankments, it provided foundational insights, as differential settlement was not measured.

With the increasing prevalence of column-supported embankments, numerous scholars have proposed various minimum heights required to achieve even settlement within embankments, referred to as the 'critical height H_{crt}', as summarized in Table 1. These tabulated critical heights have been derived from field tests (Chen et al., 2010), model experiments (Terzaghi, 1943; McGuire, 2011; Hewlett and Randolph, 1988; Horgan and Sarsby, 2002), and numerical analysis (Rui et al., 2022; Pham and Dias, 2021), ranging from 0.7 to 2.5 times the clear spacing between columns. Engineers face the challenge of balancing risk and cost when determining the appropriate critical height. To refine or rationalize this wide range, further studies are necessary to investigate soil arching within column-supported embankments.

Advancements in testing and numerical techniques have made it possible to study the kinematics of soil arching. King (King et al., 2019b) utilized synchrotron X-ray CT to obtain 3D full-field displacements within a physical model, 142 mm in diameter, comprising silica sand. Based on further studies (King et al., 2020), King recommended adopting the critical height proposed by McGuire (2011), as it was justified by both case studies and numerical analysis.

The allowable minimum embankment heights of 0.7(s-a) (BS8006, 2010), the minimum H for static load conditions $0.8(\sqrt{2}s - a)$(EBGEO, 2012), and the minimum H in CUR226(CUR226, 2010) of $0.66(\sqrt{2}s - a)$ may pose a higher risk of differential settlement compared to geometries closer to the McGuire line. This issue can be demonstrated through advanced numerical methods. For instance, Rui's analysis (Rui

* Corresponding author.
E-mail address: wadeho@icloud.com (W. He).

https://doi.org/10.1016/j.compgeo.2025.107229
Received 24 November 2024; Received in revised form 6 March 2025; Accepted 23 March 2025

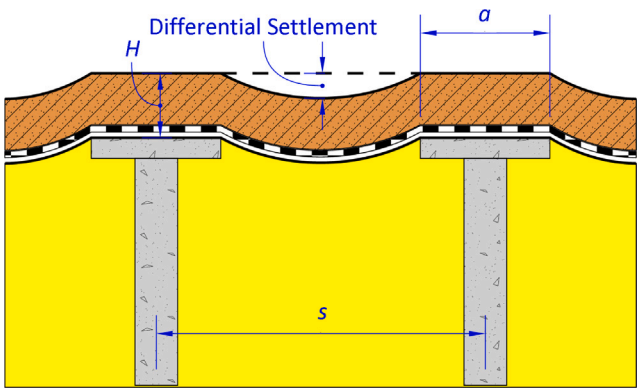

Fig. 1. Differential settlement in column-supported embankments.

Table 1
Selected proposed critical heights for column-supported embankments.

No.	Nominated critical height	Reference
1	$2.5(s-a)$	Terzaghi (1943)
2	$1.87(s-a)$	Carlsson (1987)
3	$1.4(s-a)$	Hewlett and Randolph (1988)
4	$\frac{s-a}{2}\tan 75°$	Rogbeck et al. (2003)
5	$1.545 \sim 1.92(s-a)$	Horgan and Sarsby (2002)
6	$0.5(s-a)e^{\pi\tan(\frac{\varphi}{2})}$	Naughton (2007)
7	$1.6(s-a)$	Chen et al. (2008)
8	$1.0 \sim 1.5(s-a)$	Chen et al. (2010)
9	$0.7(s-a)$	BS8006 (2010)
10	$1.15s' + 1.44d$	McGuire (2011)
11	$0.8(\sqrt{2}s-a)$	EBGEO (2012)
12	$0.66(\sqrt{2}s-a)$	CUR226 (2010)
13	$1.75(s-a)$	Rui et al. (2016)
14	$0.8(s-a)+3.0a$	Lai et al. (2018)
15	$\sqrt{2}(s-a)$	Pham and Dias (2021)
16	$1.5(s-a)$	Rui et al. (2022)

Note: s represents the center-to-center spacing of columns (i.e. piles); a denotes the (equivalent) width of the pile caps; s' is a half of diagonal center-to-center spacing of columns (i.e. piles).

et al., 2016) using the discrete element method (DEM) indicated that a punching shear mechanism occurred in embankments with heights of 0.7 to 0.8(s-a). Therefore, using the term "soil arching" to describe a punching shear mechanism may be misleading.

To further verify this finding, it is necessary to investigate the progressive development of load transfer in column-supported embankments. As a well known large strain problem, the development of soil arching in column-supported embankment includes singularity points at the corners of the columns and the propagation of shear bands through the embankment. The main disadvantages of FEM - when formulated in Lagrangian format - are related to the problem of mesh distortion. An extremely strong displacement discontinuity occurs at the edges, and tends to reduce the accuracy of finite element solutions. Even a fine mesh is constrained too much, resulting in high stress concentrations at the edges (Van Langen and Vermeer, 1991). The calculation process can even be impossible to continue when the Jacobian determinants become negative at some points of numerical integration. As a remedy, a mesh-rezoning technique can be employed in order to restore proper shapes of elements. The use of such a technique means that the fields of state variables have to be mapped from the distorted mesh to the newly generated one. This mapping is not a straight-forward task and introduces additional errors. On the other hand, the finite element method formulated in the Eulerian frame is not suitable for problems with free surfaces (Więckowski, 2004). Smith (Smith et al., 2022a) improved the finite element method by incorporating a strain-softening constitutive model, non-local integral type regularization, and the Arbitrary Lagrangian-Eulerian (ALE) method. These enhancements enable the capture of the progressive evolution of soil arching in column-supported embankments. However, in the numerical models, downwards movement of the subsoil was simulated by displacing the column upwards. This avoids numerical instability, but compromise the accuracy.

Typically, advanced methods such as material point method (MPM) or discrete element method (DEM) are required to describe the soil arching problem in column-supported embankments (King et al., 2020). DEM has been adopted by a number of researchers (Rui et al., 2022; Pham and Dias, 2021; Lai et al., 2018) to simulate soil arching behavior in column supported embankments. The notable shortcomings of DEM include: (1) due to high computational cost, analysis with real size of soil particles is nearly impossible; (2) it is challenging to simulate complex soil behaviors with contact and shear in a microscopic scale. Compared to DEM, MPM adopts the principle of continuum mechanics, which can introduce advanced constitutive models to capture nonlinear characteristics of soil, making it more suitable for analyzing soil arching within column-supported embankments.

The objective of this paper is to investigate the kinematics of soil arching using the MPM method and to revisit the critical height of column-supported embankment. Before the analysis, the MPM method is verified using existing experimental results. Based on this verification, the evolution of soil arching is studied for various embankment heights, ranging from 0.5(s-a) to 1.8(s-a). Finally, by combining data from 55 reported cases with the MPM simulation results, a formula for determining the critical height of column-supported embankments is proposed.

2. Material point method (MPM) and verification

2.1. Introduction of MPM

The MPM method is a hybrid Euler–Lagrange method that discretizes continuous material into a set of moving material points (Lagrange description), which depend on a background computational mesh (Euler description) (Sulsky et al., 1995; Ceccato et al., 2015). The Material Points (MPs) possess all the physical properties of continuous materials, such as velocities, stresses, strains, density, momentum, material parameters, and other state parameters. Unlike the traditional finite element method, the material points in MPM can move freely without being constrained by the mesh. The computational mesh is only used to solve the equilibrium equations and does not deform, as it does in the finite element method. Therefore, MPM is more effective for solving problems involving large deformations.

The computational process of MPM in each iteration cycle can be divided into four essential steps:

(1) Physical properties of the material points, such as mass, velocity, and volume, are projected onto the background mesh. This step maps the MPs' information onto the mesh for subsequent calculations (as shown in Fig. 2(a)).

(2) Equilibrium equations are solved at the nodes of the background mesh. Deformation, velocity, and acceleration fields are obtained in this step (as shown in Fig. 2(b)).

(3) The acceleration and velocity fields obtained at the background nodes are mapped to material points. The strain and strain rate at the material points are calculated using a continuum constitutive model to update stress and history variables (as shown in Fig. 2(c)).

(4) Finally, the positions of the material points are updated, and the background mesh is reset to prevent error accumulation (as shown in Fig. 2(d)).

It should also be noted that, despite the above-mentioned advantages, MPM also has some limitations. These include low mapping efficiency between material points and the background mesh, long calculation time, and difficulty in simulating complex material boundaries. Additionally, when material points move beyond the background mesh boundary, numerical oscillation problems may occur (Fern and Soga, 2016).

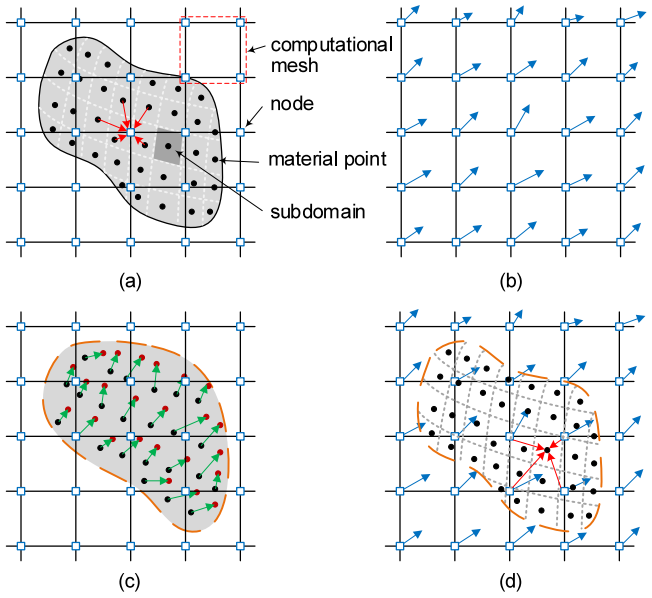

Fig. 2. Computational Framework of the Material Point Method:(a) Mapping MPs to Nodes, (b) Solving Balance Equations, (c) Mapping Velocity Field to MPs, and (d) Updating the Position of MPs.

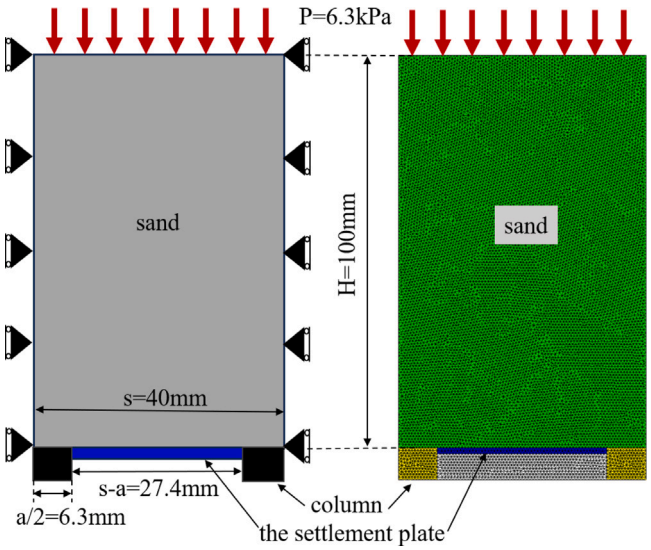

Fig. 3. MPM computational model.

Table 2
Parameters of fine sand for MPM simulation.

Parameter	Unit	Sand
Density, ρ	kN/m^3	17.56
Young's modulus, E_{ref}	MPa	40
Poison's ratio, ν	/	0.2
Peak friction angle, φ_p	°	46
Residual friction angle, φ_r	°	31.9
Peak dilatancy angle, ψ_p	°	14

2.2. Verification 1: Model tests

To demonstrate the capability of MPM for column-supported embankment analysis, a model is established to simulate a test reported in the literature (King et al., 2019b). This paper discussed a fabricated small-scale device designed to simulate column-supported embankments. The device simulated soil deformation by lowering a displacement-controlled plate, through which immobile cylindrical columns penetrate as rigid inclusions. Surrounding the columns and settlement plate is a shell made from polycarbonate, which provides confinement to fine-grained sands. The geometry of the model is summarized as below:

- Height of the model embankment = 100 mm
- Width of the column = 12.6 mm, and
- Column spacing s = 40 mm

The test was conducted with the settlement plate descending at a rate of 0.1 mm/min. The lowering of the settlement plate was paused at increments of 0.5 mm to allow for Synchrotron X-ray CT scans, ensuring that the sample was not disturbed or removed from the stages. Further details of the experimental setup and imaging technique can be found in King's paper (King et al., 2019b).

An MPM model, as shown in Fig. 3, was established using the Anura3D software (Anura3D-MPM-Research-Community, 2022) in accordance with the model test. A strain-softening constitutive model based on the Mohr–Coulomb failure criterion was adopted to simulate the embankment fill material. The soil parameters reported in the literature (Smith et al., 2022b) were used in the analysis, as summarized in Table 2. A triangular mesh with a size of 0.5 mm was introduced as the background mesh, and 3 material points were allocated to each mesh, resulting in a total of 110,792 material points. A predictive-corrective contact algorithm was employed to handle the interaction between the column and the surrounding soil. This algorithm utilizes a set of governing equations to predict the nodal velocities. Which are then corrected at the contact nodes according to the velocities and contact laws of the combined system (Bardenhagen, 2001; Ceccato et al., 2017).

The MPM analysis results, with soil settlement between columns reaching 1.0 mm, are illustrated in Fig. 4 and compared with the model test. It can be observed that the vertical displacement and maximum shear strain calculated by the MPM reasonably agree with those measured in the model test. Both sets of results indicate a constrained triangular zone between two columns where vertical displacement rapidly decreases from 1.0 mm to 0.5 mm. Outside this zone, a more evenly distributed settlement is observed, indicating less differential settlement at the road surface level. The comparison demonstrates an insignificant discrepancy between the calculated and measured settlement. On the other hand, the maximum shear strains are localized at the column-soil junctions, forming a distinct shear zone that extends upwards by approximately 13 mm, which is nearly identical to the model test results. These comparisons demonstrate the successful application of the MPM method in column-supported embankments, making it a reliable methodology for further analysis.

In addition to the 1.0 mm soil settlement achieved in the model test, the MPM analysis was extended to cover scenarios with larger soil settlement. The results demonstrate that soil arching fully develops with 1.0 mm of soil settlement. When the embankment is of sufficient height, larger soil settlement between columns does not trigger differential settlement at the top of the embankment, although it does induce minor total settlement. Therefore, the 1.0 mm soil settlement is reasonable to adopt in the numerical analysis to study the kinematics of soil arching for the geometry of the model test.

2.3. Verification 2: Field tests

MPM was further validated by modeling a field test using 3D cell models. The field tests were conducted on a 126 m-long trial embankment on the TJ highway, China (Chen et al., 2010). The embankment was 6.0 m high with a road width of 26 m. The ground profile at the site consists of an approximately 3 m-thick crust (clay), a 16 to 17 m-thick soft soil layer, and a 15 to 17 m-thick pebble layer, underlain by

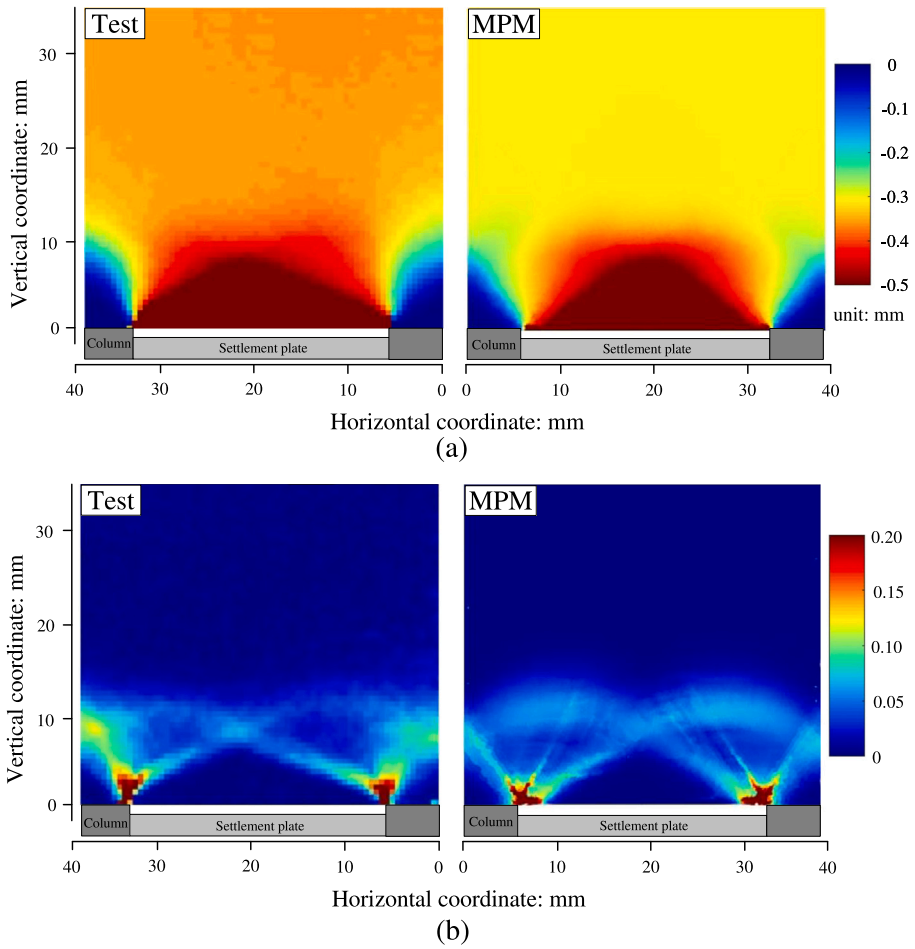

Fig. 4. Comparison between the model test and MPM analysis:(a) vertical displacements, (b) maximum shear strains.

Table 3
Summary of three testing scenarios in TJ Highway.

Scenario	H (m)	d (m)	L (m)	s (m)	a (m)
G1	6.0	0.4	20	2.5	1.3
G2	6.0	0.4	20	3.0	1.6
G3	6.0	0.4	20	2.0	1.0

Note: H = embankment height; d = pile diameter; L = pile length; s = pile center to center spacing; and a = pile cap width.

tuff. Prestressed pipe piles, 0.4 m in diameter, were driven through the soft soil to the dense pebble layer. The pipe piles were installed in a square pattern with center-to-center spacing of 2.0 m, 2.5 m or 3.0 m. To mitigate potential differential settlement, pile caps measuring 1.0 m×1.0 m, 1.3 m×1.3 m, or 1.6 m×1.6 m were placed on top of the pipe piles. The embankment and pile arrangement are illustrated in Fig. 5.

Three scenarios were tested in the field, combining various pile spacings and pile cap sizes. The details of these three test scenarios are summarized in Table 3. For each scenario, two settlement plates and nine earth pressure cells were installed after the pile caps were constructed to measure settlement and vertical earth pressure at the pile cap level. The locations of these settlement plates (S1-S2) and earth pressure cells (E1-E9) are shown in Fig. 5(b). The average earth pressure and settlement on the pile caps and subsoil reported in the paper have been extracted and modeled herein for 3D verification.

The three scenarios were simulated using 3D unit cell models with MPM. The typical geometry of the models is illustrated in Fig. 5(c). The soil parameters provided in the original paper were adopted for the analysis.

The calculated earth pressure and settlement were quantitatively compared to the measured values, as illustrated in Fig. 6(a) and (b), respectively. In general, the results demonstrated good agreement in both earth pressure and settlement, with minor discrepancies at certain stages. Overall, the MPM analysis captured the main trend in the development of settlement and earth pressure, indicating the successful application of the MPM method to 3D problems. The 3D verification further confirmed that MPM is a reliable methodology for column supported embankments.

3. Kinematics of soil arching in column-supported embankments

Shear patterns for various embankment heights and interactions with adjacent columns of different sizes and spacings are investigated using MPM, as follows.

3.1. Shear patterns

MPM models with various embankment heights are analyzed in this section. Using the same column size (a = 12.6 mm) and spacing (s-a = 27.4 mm), embankment heights ranging from 19.2 mm (i.e. H = 0.7(s-a)) to 38.4 mm (i.e. H = 1.4(s-a)) were modeled in Anura3D. Only the results for embankment with heights from 0.7(s-a) to 1.2(s-a) are plotted in Fig. 7, since non-significant changes in vertical displacement

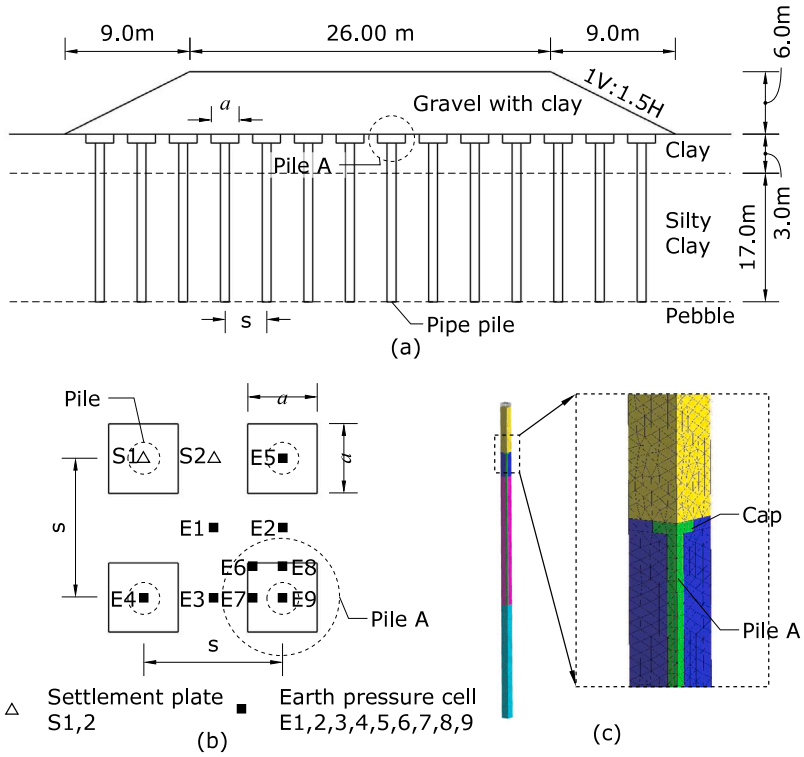

Fig. 5. The field test arrangement and the corresponding MPM model: (a) cross-section; (b) pile and cap arrangement; (c) MPM model.

and shear stress were observed when the embankment height exceeded 1.2(s-a).

As illustrated in Fig. 7, the bearing mechanism of a low embankment with a height of 0.7(s-a) is predominately characterized by a punching shear pattern, which includes two inclined shearing zones develop from the edges of the columns to the embankment surface. Significant differential settlement can be observed at the top of the embankment. As the embankment height increases, a localized shear zone emerges above the columns starting at an embankment height of 0.8(s-a) and gradually develops into an invert general bearing failure pattern. When the embankment height exceeds 1.2(s-a), the punching shear pattern is barely observable in the shear strain field. At the same time, the differential settlement at the top of the embankment is insignificantly reduced, as shown in Figure fig7: various height results(e). In summary, punching shear failure dominates in low embankments (height no greater than 0.7(s-a)), and the inverted general bearing pattern governs in high embankments (height greater than 1.2(s-a)). Embankments with heights between 0.8(s-a) and 1.1(s-a) represent the transition from a punching shear to an inverted general bearing pattern.

3.2. Interaction with adjacent columns

The spacing between columns is another factor that can alter the shearing pattern within an embankment, even with sufficient embankment height to avoid the punching shear pattern. Recent research (Smith et al., 2022b) indicates the existence of a critical column spacing, s_{int}, beyond which the Prandtl radial shear zone between adjacent columns no longer interacts. King (King et al., 2019a) distinguished four cases based on s_{int} and the column spacing, s. These cases can be illustrated using MPM, although they may not be easily simulated by FEM. Some extreme cases, such as s = 21a, were modeled herein to illustrate the interaction of adjacent shear zones, as shown in Fig. 8. The embankment height adopted in the models is consistently H = 1.2(s-a), and the graphical outputs of those larger models (i.e. with high embankment) were trimmed to 100 mm to facilitate comparison.

As observed in Fig. 8, increasing the column spacing reduces the interaction between adjacent shear zones. The shear bands in embankments with smaller column spacing (e.g. s = 3.2a) exhibit an inverted general bearing pattern, with the maximum shear strain developing along the boundary of each zone. As the column spacing increases, the shear strain intensifies at the top of the columns and decreases between the two columns. It appears that the difference in shear strain becomes significant when s> 5a. Nonetheless, the interaction with adjacent columns can still be observed until it becomes completely independent at a column spacing s = 21a. Simultaneously, the analysis shows that a larger spacing does not cause differential settlement but results in greater total settlement at the top of the embankment. It is anticipated that the columns can be effectively ignored with adequate spacing.

On the other hand, the clearance between columns can be reduced by introducing pile caps, which is an efficient way to mitigate the risk of differential settlement at the top of low embankments. To investigate this effect, with the same clearance of 27.4 mm, column sizes ranging from 12.6 mm to 50.4 mm are modeled in MPM, and the graphical outputs are shown in Fig. 9. The results indicate that column size can alter the shear pattern within embankments. With larger column sizes, the inverted general bearing pattern is still visible, but the shear strain primarily develops along the shear bands from the edges of the columns, inclining up to the central line, and decreases in the rest of zone. This suggests that soil between two columns is spaced sufficiently close to each other.

The observation above is generally consistent with that reported in the literature (King et al., 2019a). Nonetheless, the transitional case is observed over a wider range of column spacing rather than only at $s = s_{int}$. Therefore, the four cases of interaction may be modified as shown below and illustrated in Fig. 10.

(1) Case A: $s \leq s_{min}$. When columns are spaced sufficiently close to each other, the maximum shear strain localizes in a triangular zone

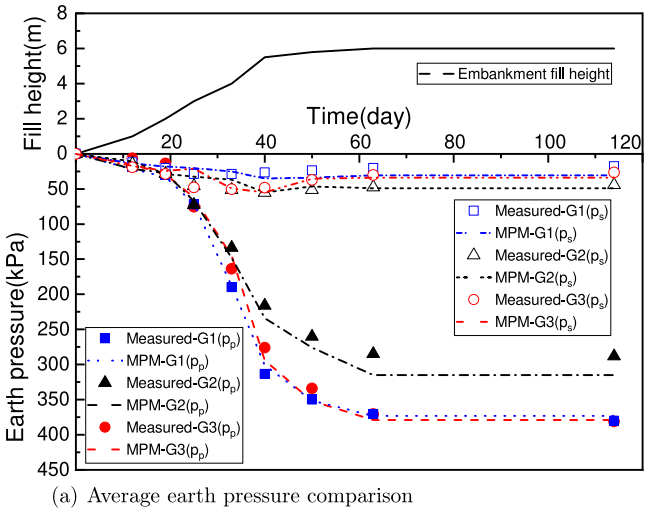

(a) Average earth pressure comparison

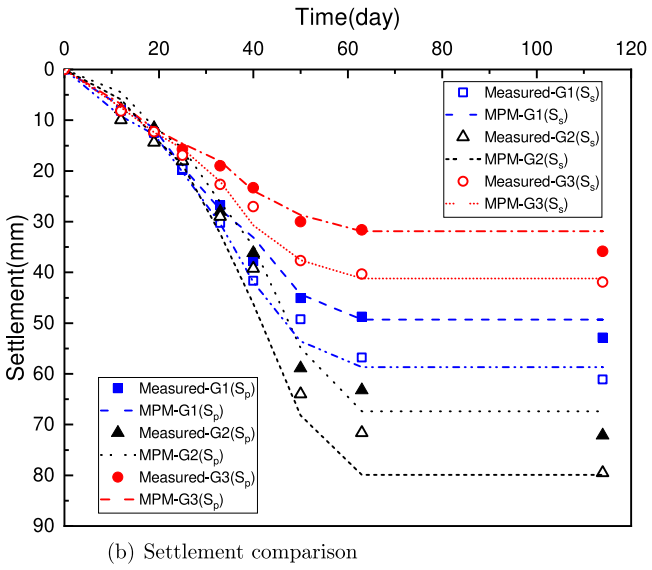

(b) Settlement comparison

Fig. 6. Comparison of calculated to the measured earth pressure and settlement.

between the columns(as shown in Fig. 10(a), and the system behaves as a single foundation. The spacing at which this case occurs is observed to be $s_{min} = 2a$, in accordance with the MPM results.

(2) Case B: $s_{min} < s \leq s_{cr}$. A clear inverted bearing mechanism is observed. The active zone (zone I), Prandtl radial shear zone (zone II), and Rankine passive zone (zone III) are segregated by the shear bands, as illustrated in Fig. 10(b). The maximum shear strain appears in all the shear bands, indicating continuous involvement of the soil between columns in the soil arching effect when the spacing is below a critical value, s_{cr}. The MPM analysis demonstrated that the critical value is between 5a and 8a, beyond which the columns may start punching into the embankment.

(3) Case C: $s_{cr} < s \leq s_{int}$. The inverted bearing mechanism can still be observed; however, the maximum shear strain is predominantly localized in a triangular zone above the columns, and the shear strain becomes less significant farther from the columns. The vaguely defined Rankine passive zone and the Prandtl radial shear zone interact between adjacent columns.

(4) Case D: $s > s_{int}$. When s-a > 21a, the shear zones of adjacent columns are separated, and no interaction can be observed, although such a large pile spacing is rarely adopted in ground improvement design.

Differentiating the interaction cases helps engineers choose a reasonable column spacing in design based on the bearing mechanism of column-soil system. For an economic design, the column spacing is recommended to be limited between s_{min} and s_{cr} (i.e. 2a to 5a according to this research). The same rule applies when pile caps are used. Adopting a smaller spacing may be unnecessarily costly, while using a larger spacing makes it difficult to form a composite system.

4. 3D MPM analysis of a column-supported embankment

A series of 3D cell models was established in alignment with a real project (He et al., 2023) to study effects such as underlying soft ground and 3D geometry.

4.1. Model and soil parameters

The project involves upgrading an existing motorway in Southeast Queensland, Australia. The typical soil profile at the site consists mainly of three strata: approximately 3 meters of very loose to loose sand, followed by up to 10 meters of soft to firm clay or silty clay, overlying residual soil or weathered rock. The paper indicates that the existing embankment was treated in the 1980s using preloading/surcharge with wick drains. For this road widening project, one effective treatment method is the use of rigid inclusions. Controlled Modulus Columns (CMCs), 450 mm in diameter and extending approximately 0.5 m into the residual soil or weathered rock, are assumed to be used as ground treatment beneath the embankment. Column spacings ranging from 2D to 8D, with embankment heights from 0.5(s-a) to 1.8(s-a), were analyzed in this study. A typical MPM model based on the ground profile is illustrated in Fig. 11.

In light of several previous studies (Han et al., 2007; Yu et al., 2016; Wijerathna and Liyanapathirana, 2020; Pham and Dias, 2021), the Mohr–Coulomb and a linear elastic model were employed to simulate the soils and columns, respectively. A load of 20 kPa is adopted in the analysis to simulate vehicle loads on pavements, consistent with the literature (Smith et al., 2022b). The parameters used in the analysis are listed in Table 4.

Displacement contours of the column-supported embankment were derived from the analysis results. Fig. 12(a) and (b) show the side and top views of the displacement contours for a column-supported embankment with a column spacing of s=5d and varying embankment heights. For smaller embankment heights, the tops of the embankments exhibit more significant differential settlement, as indicated by the non-uniform colors in Fig. 12(a) and (b). In these figures, blue represents low settlement, while red represents high settlement. Settlement becomes reasonably uniform when the embankment height exceeds 1.3(s-a). Consequently, the critical height for the column-supported embankment in this case is considered to be 1.3(s-a), warranting further investigation.

The settlement at the top of the embankment for each embankment height was extracted and plotted in Fig. 12(c). This provides a quantitative representation of differential settlement, showing that settlement gradually stabilizes as the embankment height increases from 0.5(s-a) to 1.8(s-a). Meanwhile, the differential settlement decreases from 1.5% to nearly 0%. The embankment heights corresponding to differential settlements of 0.5% and 0.1% are 0.9(s-a) and 1.2(s-a), respectively.

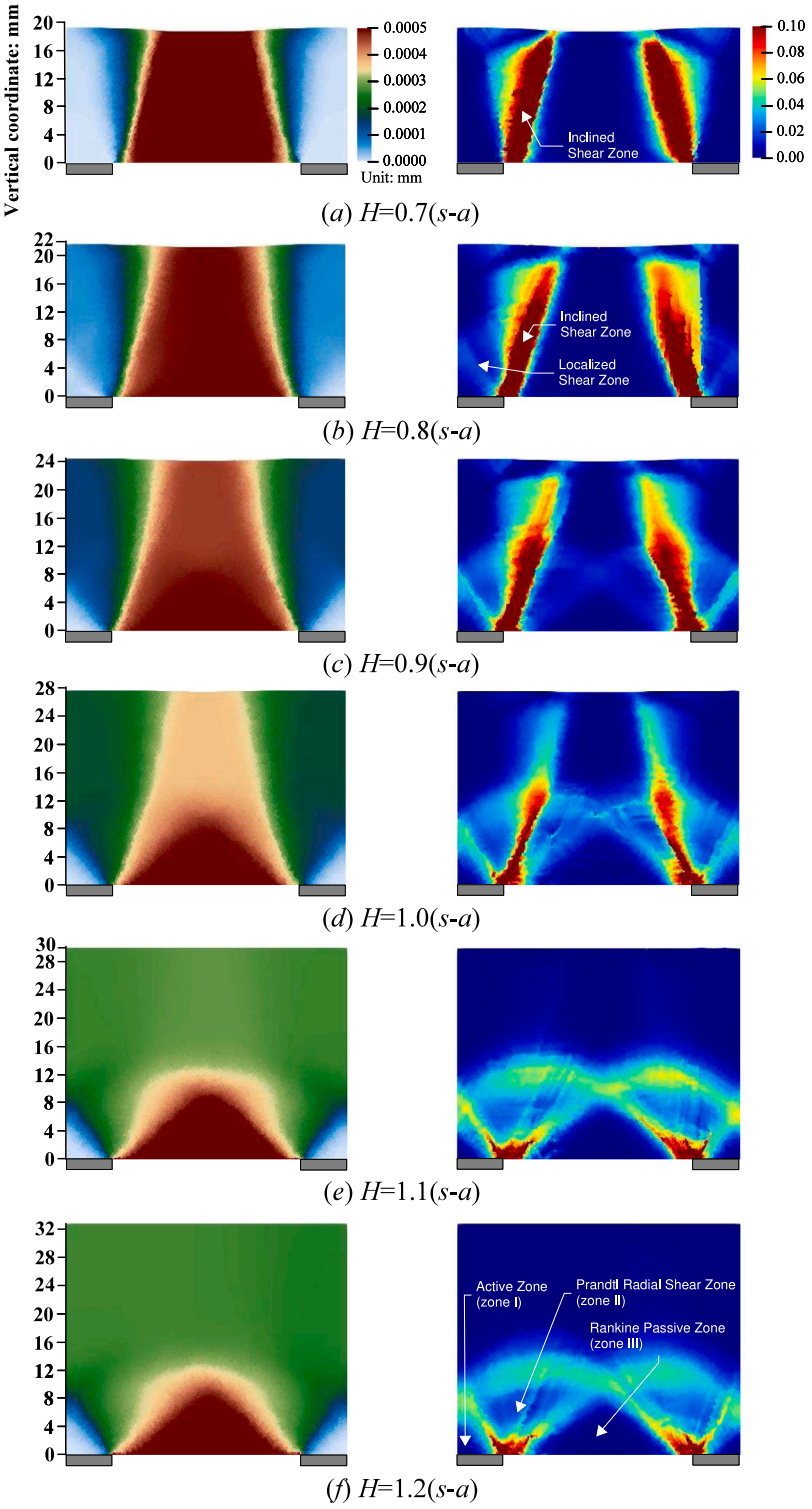

Fig. 7. Vertical displacement and maximum shear strain within embankment of heights H = 0.7 to 1.2(s-a).

Table 4
Soil and rock parameters.

Materials	γ (kN/m^3)	c (kPa)	φ (°)	ψ (°)	E (MPa)	ν
Embankment FILL	20	5	30	0	21	0.3
Stiff CLAY	20	3	28	0	20	0.3
Loose SAND	17	0	30	0	10	0.3
Soft CLAY	16	1	24	0	10	0.3
Very loose SAND	16	0	28	0	8	0.3
Extremely weathered ROCK	23	100	35	5	100	0.2

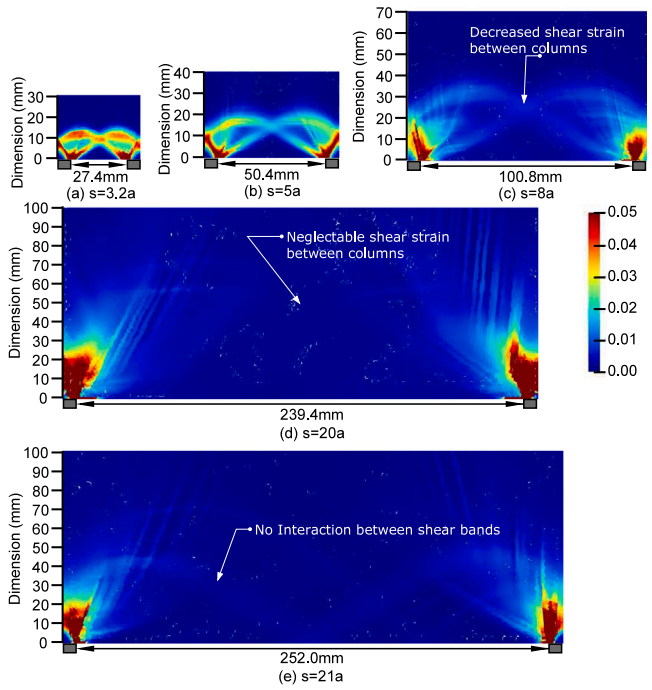

Fig. 8. The Maximum Shear Strain Contours illustrating the Interaction with Adjacent Columns at various Spacings.

With column spacings of 2d to 4d or 6d to 8d, the settlement at the top of the embankment and within the embankment exhibit a similar trend; therefore, these results are not replicated here.

4.2. Strain and stress within the embankments

The soil arching effect in column-supported embankments can be characterized by the shear strain and principal stresses patterns within the embankment (King et al., 2019b; Smith et al., 2022a). Accordingly, the contours of maximum shear strain and vertical stress for an embankment with a column spacing of 5d and varying heights are plotted in Fig. 13.

The strain and stress contours indicated in Fig. 13 are generally consistent with those in Fig. 7 predominately showing three types of morphology:

(1) Punching shear (0.5(s-a) to 0.7(s-a)): In low embankment heights, a shearing band extending from the edge of the columns to the surface of the embankment is clearly observed, exhibiting a morphology similar to that of a punching shear failure. The vertical stress at shallow depths between two columns is significantly increased. This observation is consistent with the experimental results reported by Brzeziński and Michalowski (2021).

(2) Transition from punching shear to soil arching (0.7(s-a) to 1.2(s-a)): As the embankment height increases, the shearing band no longer penetrates through the embankment but bifurcates towards adjacent columns. The bifurcation can be observed in the cases of 0.9(s-a) and 1.0(s-a); however, the higher vertical stress can still be observed at shallow depths between the columns, indicating load redistribution due to shearing.

(3) Soil arching (> 1.2(s-a)): When the embankment height exceeds 1.2(s-a), the shearing band develops only towards adjacent columns, forming an arch-like shape. No stress redistribution can be observed at shallow depths within the embankment, with negligible differential settlement at the top of the embankment.

For column spacing between 2d and 4d, or 6d and 8d, similar strain and stress contours are observed; therefore, they are not replicated here.

4.3. Critical height of embankments

The critical height of embankments, above which no significant differential settlement is observed, as proposed by various researchers, is further discussed in this paper based on MPM analysis and reported testing results, including model test and real cases. The differential settlement at a certain level within embankments can be quantified

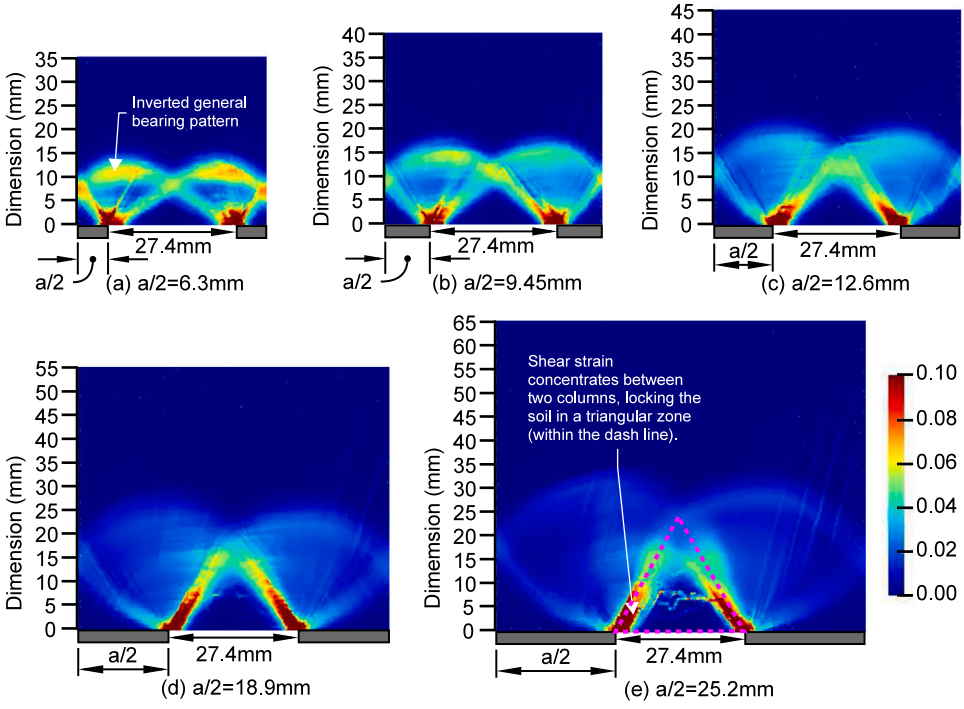

Fig. 9. The Maximum Shear Strain Field illustrating the Interaction with Adjacent Columns of Various Sizes.

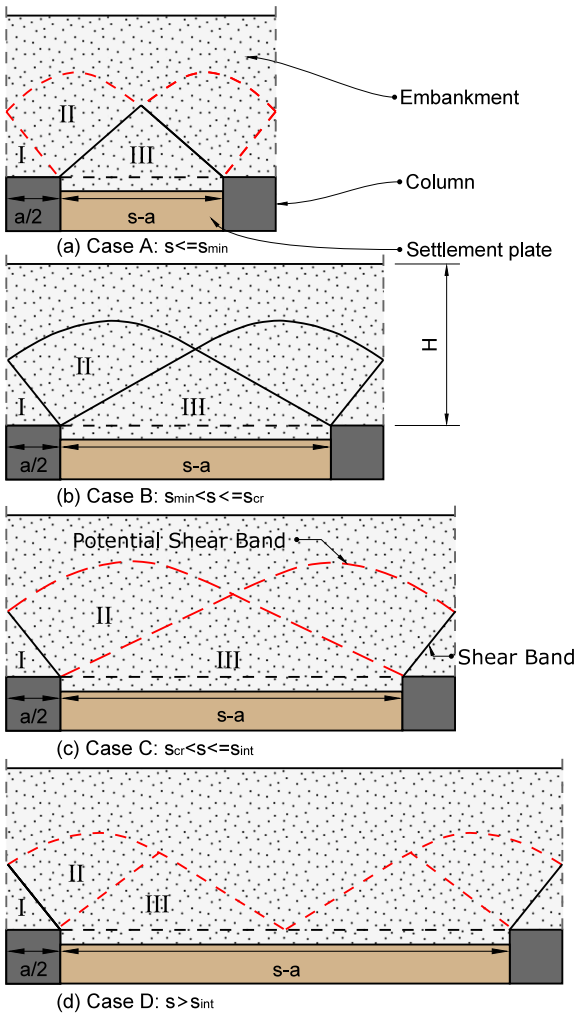

Fig. 10. Schematic Diagram illustrating the Influence of Column Spacing on Embankment Deformation.

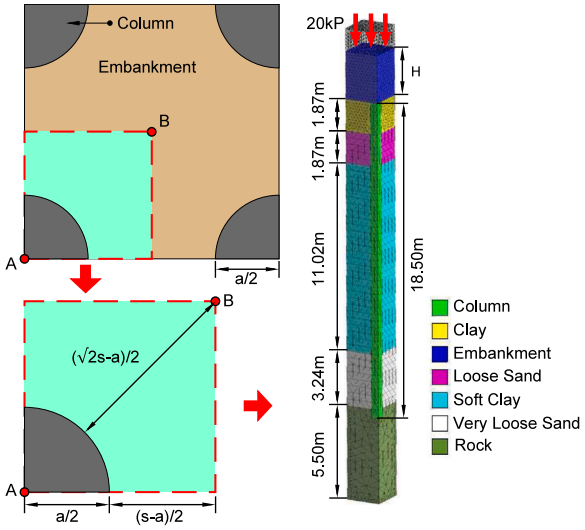

Fig. 11. Illustration of the 3D MPM model.

by the ratio of the settlement difference to the distance between two points.

The maximum differential settlement typically occurs between the top of the columns and the midpoint between the columns. Taking the grid pattern as an example (Fig. 14), the differential settlement, δ, is defined as the difference between the settlement S_p at the center of the column (point A) and the settlement S_s at the midpoint between columns (point B), divided by the distance between point A and point B: $L_{AB=s'+d/2}$.

$$\delta = \left(S_s - S_p\right)/L_{AB} \tag{1}$$

A total of 85 MPM models with column spacings ranging from 2d to 8d were analyzed, and the differential settlement δ at the top of the embankments are illustrated in Fig. 15.

Fig. 15 shows that the differential settlement at the top of the embankment decreases linearly with increasing embankment height in the initial stage. Subsequently, the relationship becomes nonlinear, with the differential settlement dropping below 0.3% and gradually approaching zero. Generally, larger column spacing requires a higher embankment to achieve the same level of differential settlement.

The normalized embankment heights required to achieve differential settlements of 0.1% to 0.5% are tabulated in Fig. 15, assuming a typical column size of a = 0.45 m. It is observed that the differential settlement of column-supported embankments with column spacings of 2d to 8d is typically less than 0.1% when the embankment height exceeds 1.2(s-a). If the criteria is relaxed to 0.3% or 0.5%, the required embankment height decreases to 0.7(s-a) to 1.0(s-a), depending on the column spacing. These embankment heights slightly exceeds the 0.7(s-a) recommended in the British Standard (BS8006, 2010), which may warrant further review. Conversely, the 1.4(s-a) recommended by Hewlett and Randolph (1988), adopted in the Chinese Standard (JTG-T-D31-02-2013, 2013), is considered conservative and on the safe side.

In addition to the 1.4(s-a) criterion in the Chinese codes, McGuire (2011) proposed a dimensionless critical height of embankments (H_{crit}), as expressed in Eq. (2).

$$\frac{H_{crit}}{d} = 1.15\frac{s'}{d} + 1.44 \tag{2}$$

Refer to Fig. 14 for the definitions of s' and d.

This critical height was validated by McGuire (2011) through numerous experimental results, and the McGuire line for critical height has been widely accepted by engineers (King et al., 2020). However, there is a notable drawback when applying McGuire line to design: Eq. (2) suggests that critical height monotonically increases with column diameter. This can lead to unreasonable results, particularly when pile caps are used to reduce differential settlement.

For example, consider an embankment with a minimum height of 2.13 m (i.e. H = 2.13 m), supported by columns with a diameter of 0.45 m and a spacing of 2.25 m (i.e. d = 0.45 m and s = 2.25 m). The dimensionless height and spacing are calculated as $s'/d = 3.04$ and $H/d = 4.73$, which is plotted as a hollow circle (i.e. Scenario 1) in Fig. 16. Comparing this to the McGuire line and the equation $H = 1.4(s-a)$ adopted in the Chinese Standard (JTG-T-D31-02-2013), Scenario 1 falls below both criteria, indicating a high risk of differential settlement.

A typical solution in this case is to introduce a larger pile cap(say, 1m×1 m) at the top of the columns to reduce the spacing between them. The new dimensionless height and spacing are then calculated as $s'/d = 0.91$ and $H/d = 1.88$, plotted as a hollow triangle (i.e. Scenario 2) in Fig. 16. Contrary to expectations, Scenario 2 moves further away from the McGuire line compared to Scenario 1, implying a higher risk when pile caps are used. The issue arises due to the monotonically increasing relationship between critical height and column diameter in the McGuire equation (i.e. (2)).

On the other hand, the criterion $H = 1.4(s-a)$ demonstrates reasonable results. Converting this equation to a relationship between

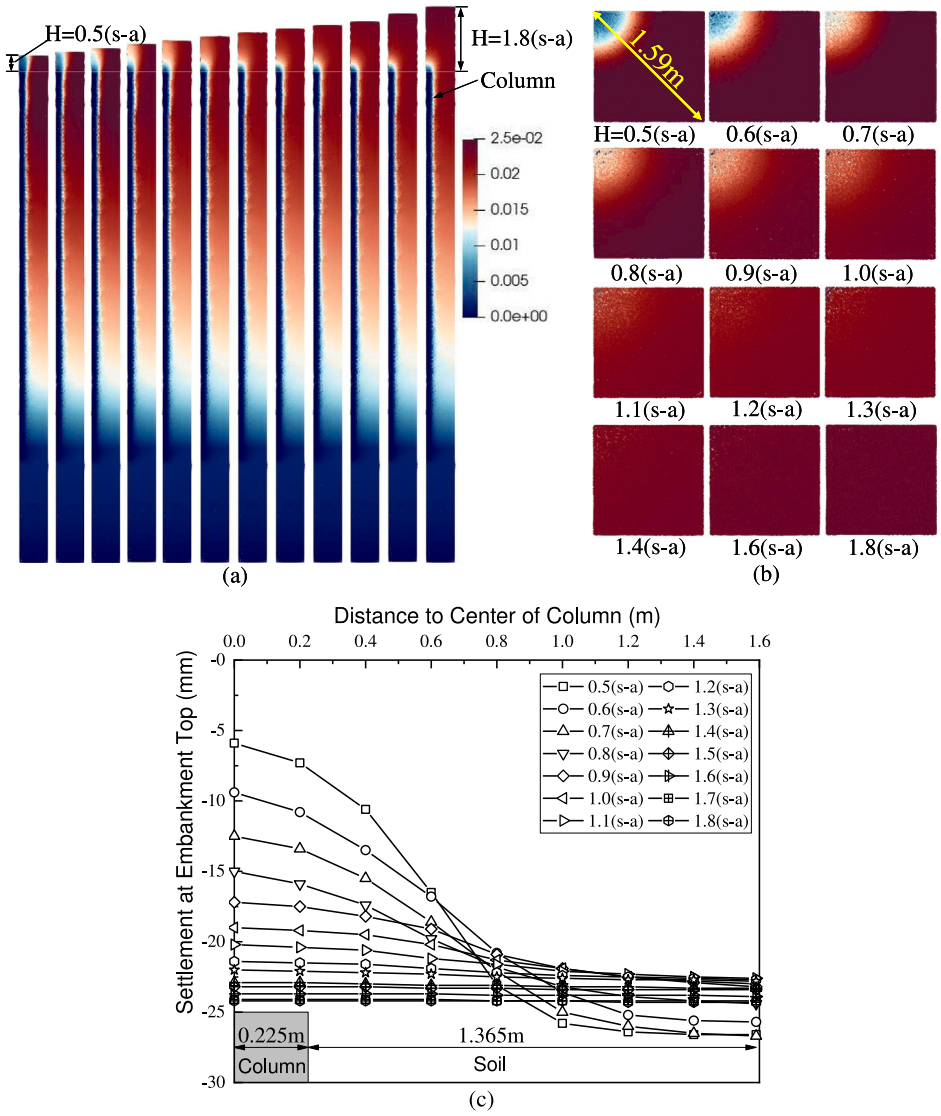

Fig. 12. Settlement Deformation Diagram with Column Spacing of 5d : Schematic representation of embankment settlement for fill heights H = 0.5 to 1.8 (s-a): (a) Front view, (b) Top cloud view, (c) Settlement curve of soil at the top of the embankment.

s'/d and H/d yields $H_{crit} = 1.98s' - 0.25d$, which shows a monotonically decreasing relationship between critical height and column diameter. As a best-fitted line, the McGuire line may be appropriate for higher value of s'/d, where variations in column diameter have a negligible impact. However, for smaller values of s'/d, particularly when pile caps are used, applying the McGuire line in engineering practice may be misleading.

To further investigate the critical height of embankments, the testing results employed by McGuire (Cases 1 to 46, as shown in Fig. 17) were plotted alongside nine additional field tests reported by researchers in China (Cases 47 to 55, as shown Fig. 17 and summarized in Table 5). The additional field tests include: a field monitoring in Jinan, Shandong Province (the Case 47) (Zhang et al., 2021), the Wuhan-Guangzhou highspeed railway (the Case 48) (Zhang et al., 2010), the Shen-Su-Zhe-Wan Highway (Shanghai-Jiangsu-Zhejiang-Anhui) (the Case 49) (Xu et al., 2009), the Tai-jin Highway (Taizhou-Jinyun, Zhejiang Province) (the Case 50) (Xu et al., 2008), the Zhe-Bei highway in Zhejiang Province (the Case 51) (Zuo et al., 2013), a highway in a Northern Suburb of Shanghai (the Case 52) (Fei and Liu, 2009), the Xing-Shan Highway in Guangdong Province (the Case 53) (Ye et al., 2021), the highspeed railway from Kunming, Yunnan Province to Nanning, Guangxi Province (Case 54) (Pan et al., 2022), and the Xiong'an New Area Highway in Hebei Province (the Case 55) (Yang et al., 2022). These case studies supplement field observations for s'/d values between 0.44 and 3.74, with the majority falling below 2 (i.e. $s'/d \leq 2$). A summary of each case is provided in Table 5.

All the available data have been converted into a relationship of H/d versus s'/d and plotted in Fig. 17. Cases where differential settlement occurred are represented as solid squares, which are expected to lie below the proposed critical line. In contrast, cases where no differential settlement was observed are located above the proposed critical line.

The MPM analysis results are also included in Fig. 17 and are divided into two groups based on a differential settlement threshold of 0.1%. The red crosses in Fig. 17 represent cases where critical heights have been interpreted by researchers, predominately based on stress changes measured within the embankments.

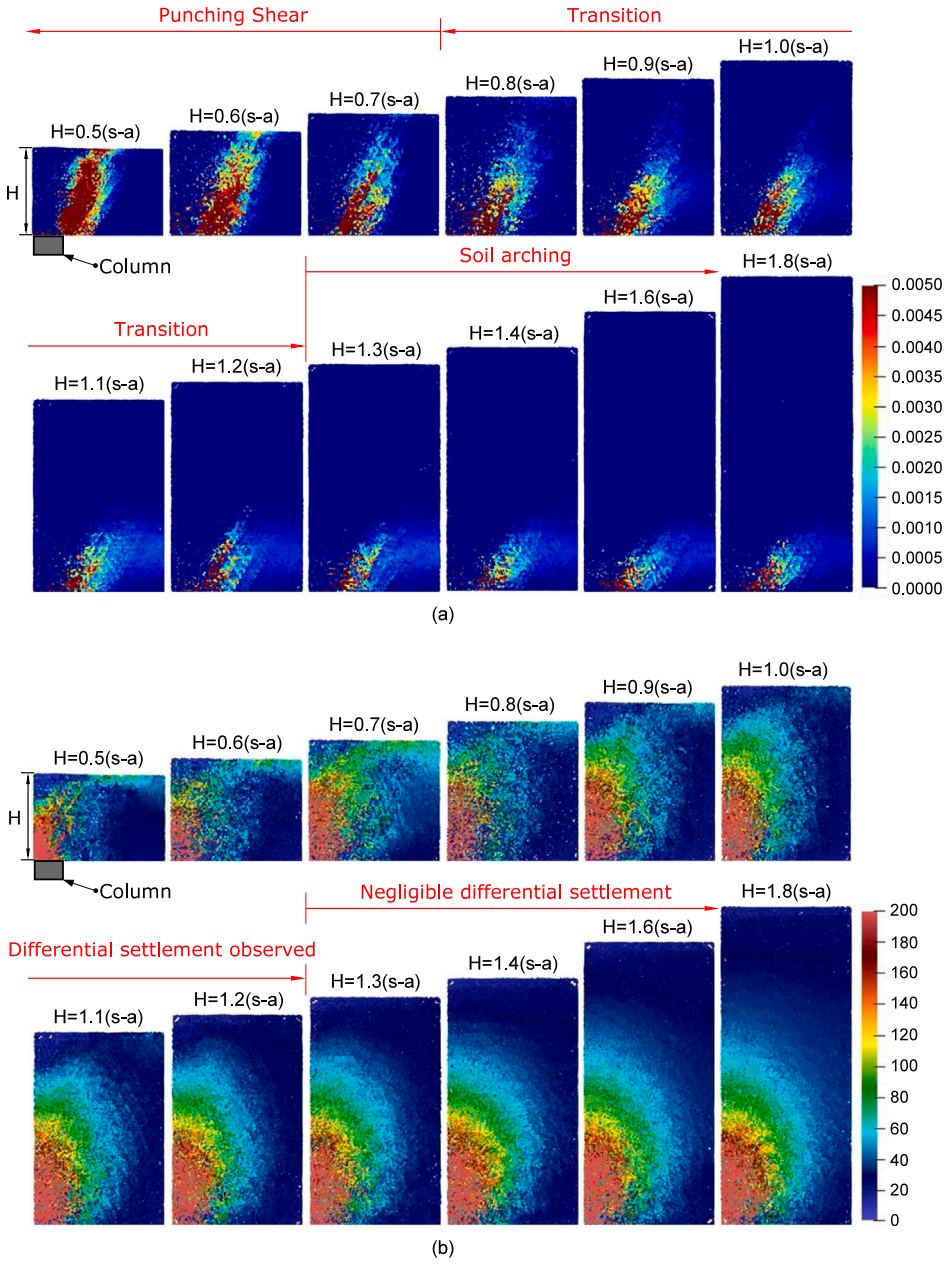

Fig. 13. Shear Strain and Vertical Stress Contours within an Embankment: (a) Maximum shear strain, (b) Vertical stress.

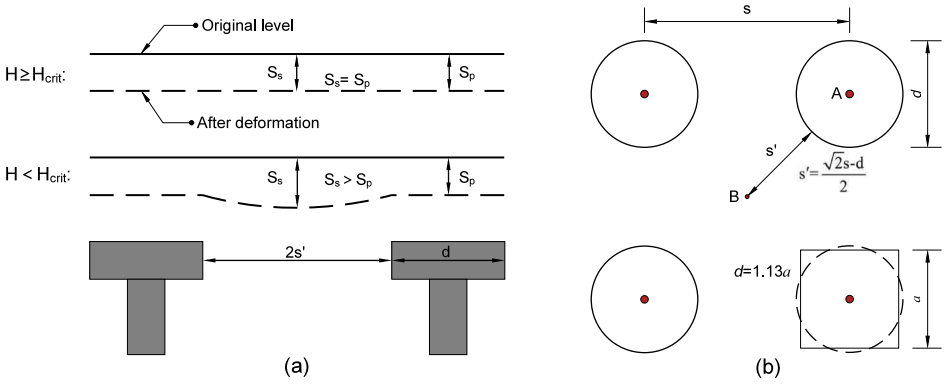

Fig. 14. Differential settlement within a column-supported embankment, (a) differential settlement above and below the equal settlement surface, (b) plan view illustrating conversion of parameters.

Table 5
Summary of additional field testing results: Case 47 to 55.

Case	s (m)	d (m)	H (m)	H_{crit}(m)	s′/d	H_{crit}/d
47	1.8	1.36	5.6	1.47	0.44	2.00
	2.0	1.00	3.5	0.90	0.91	0.90
48	2.0	0.50	3.5	3.80	2.33	1.90
	3.0	0.50	3.5	5.20	3.74	2.60
49	2.0	1.02	4.0	1.19	0.89	1.21
	2.5	1.13	4.0	1.53	1.06	1.725
50	2.5	1.47	4.5	0.98	0.70	1.44
	3.0	1.81	4.5	1.08	0.67	1.96
	2.0	1.13	4.5	0.88	0.75	1.00
51	1.35	0.57	4.15	1.89	1.19	1.07
52	3.0	1.00	5.6	/	1.62	/
53	2.6	1.36	7.4	/	0.86	/
	2.6	1.36	8.6	/	0.86	/
54	1.8	1.00	10.53	1.12	0.77	1.12
	1.8	1.00	9.82	2.40	0.77	2.40
55	2.0	1.13	7.2	1.50	0.75	1.33
	2.2	1.13	7.3	1.50	0.88	1.33
	2.0	1.13	5.3	/	0.75	/
	2.2	1.13	5.1	/	0.88	/

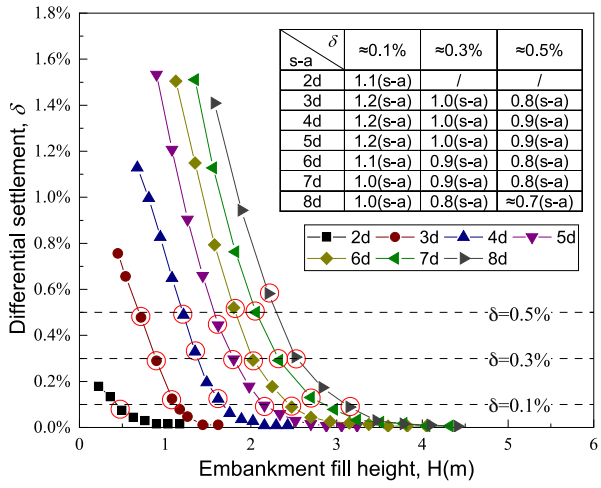

s-a \ δ	≈0.1%	≈0.3%	≈0.5%
2d	1.1(s-a)	/	/
3d	1.2(s-a)	1.0(s-a)	0.8(s-a)
4d	1.2(s-a)	1.0(s-a)	0.9(s-a)
5d	1.2(s-a)	1.0(s-a)	0.9(s-a)
6d	1.1(s-a)	0.9(s-a)	0.8(s-a)
7d	1.0(s-a)	0.9(s-a)	0.8(s-a)
8d	1.0(s-a)	0.8(s-a)	≈0.7(s-a)

Fig. 15. Differential settlement at top of embankment with various heights and column spacings.

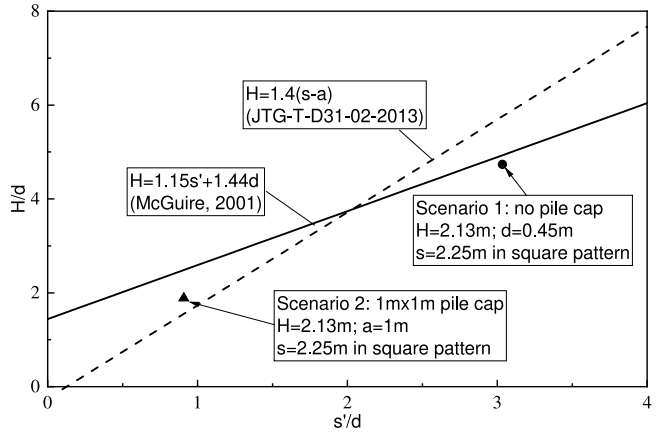

Fig. 16. Differential settlement at top of embankment with various heights and column spacings.

Five criteria proposed by different researchers or adopted in codes from various countries are plotted in Fig. 17. All five criteria are linear, with the lower bound at H = 0.7(s-a) in BS8006. Since a number of cases above this line have reported differential settlement (i.e. failed cases), and numerical analysis by King (King et al., 2020) indicated that stress development largely follows a punching shear mechanism, using H = 0.7(s-a) in design practice is both confusing and misleading. The criteria proposed in CUR226(CUR226, 2010) and EBGEO (EBGEO, 2012) cover more failed cases, but they can be further optimized based on numerical analysis and field testing results. Although the drawback of the McGuire line (McGuire, 2011) for the lower range of s'/d is notable, it is based on a large database of experimental observations and aligns well with numerical analysis results for higher values of s'/d ($s'/d > 2$).

As shown in Fig. 17, at the lower end of s'/d, several cases without differential settlement fall below the McGuire line, suggesting that its applicability in this range should be revisited. Consistent with the case studies, MPM analysis results for $s'/d \leq 2$ also indicate a smaller critical height than that suggested by the McGuire line. Among the proposed criteria, the H = 1.4(s-a) criterion adopted in the Chinese Standard (JTG-T-D31-02-2013, 2013) appears more suitable for $s'/d \leq 2$, as shown in Fig. 17.

Based on the above observations, the authors believe that the actual critical height line in the H/d - s'/d axis should be nonlinear and, therefore, cannot be described by a single linear equation. Deriving an analytical solution for this nonlinear criterion is challenging; however, it can be approximated using a polyline. Consequently, a combination of the McGuire line for s'/d>2 and H = 1.4(s-a) for $s'/d \leq 2$ may be more appropriate. Since H = 1.4(s-a) can be rewritten as H = 1.98s'-0.25d, the formula can be modified accordingly, as shown in Eq. (3):

$$\frac{H_{crit}}{d} = \begin{cases} 1.98\frac{s'}{d} - 0.25 & (\frac{s'}{d} \leq 2) \\ 1.15\frac{s'}{d} + 1.44 & (\frac{s'}{d} > 2) \end{cases} \quad (3)$$

Eq. (3) shows good agreement with test results, though further verification through field studies is required.

5. Conclusions

The column-supported embankments were analyzed using the MPM method to study the soil arching effect within the embankments and to determine the critical height above which the risk of differential settlement can be eliminated. Based on the numerical analysis and experimental results from other studies, the following conclusions can be drawn:

(1) The Material Point Method (MPM) demonstrates a natural capability for analyzing large-strain problems in geotechnical engineering.

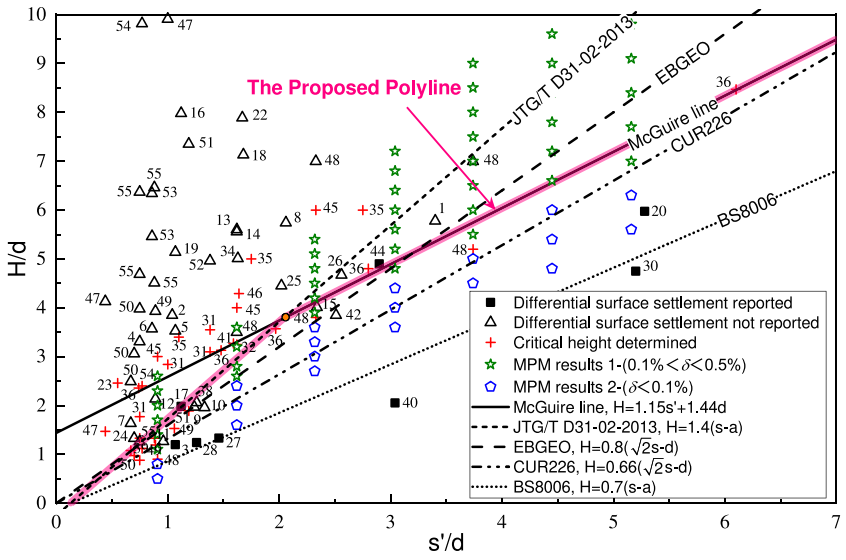

Fig. 17. Normalized embankment height versus spanning ratio for 3D unit cells.

It effectively captures the soil arching effect within column supported embankments. This has been validated by comparing the numerical analysis with model test results.

(2) The shearing pattern within the embankment varies with embankment height. A punching shear pattern dominates when the embankment height $H \leq 0.7(s-a)$, transitioning to an inverted general bearing pattern when $H > 1.2(s-a)$. The inverted general bearing pattern interacts with adjacent columns unless the columns spacing $s \geq 21a$. Four interaction cases were identified and summarized in the paper.

(3) The analysis results indicates that differential settlement at the top of the embankments decreases linearly with increasing embankment height during the initial stage and becomes nonlinear as the height reaches 0.8(s-a) to 1.0(s-a). It then gradually approaches zero. Differential settlement falls below 0.1% when the embankment height reaches 1.2(s-a) and stabilizes thereafter. The authors support the view that the minimum requirement of H = 0.7(s-a) specified in the British Standard BS8006 may be overly optimistic for engineering practice.

(4) Case studies demonstrated that the McGuire equation can lead to unreasonable results, particularly when pile caps are used to reduce differential settlement (typically with smaller s'/d). The issue arises due to the monotonically increasing relationship between critical height and column diameter in the McGuire equation. To address this, additional case studies from China and numerical results from MPM were analyzed alongside previously available data from McGuire's phD thesis. The analysis suggested that the actual critical height line is likely nonlinear in nature. Based on the findings, the McGuire line is appropriate for $s'/d \geq 2$, while $H_{crit} = 1.4(s-a)$, rewritten as $H_{crit} = 1.98s'/d - 0.25$, may be more suitable for s'/d< 2. Therefore, a polyline is proposed to approximate the actual critical height line in the H/d - s'/d axis.

(5) The proposed critical height line should be further verified through field studies. Additionally, developing and theoretically supporting its potential nonlinear form would be beneficial for design practice.

CRediT authorship contribution statement

Wei He: Writing – review & editing, Visualization, Supervision, Resources, Project administration, Methodology, Funding acquisition, Conceptualization. **Kaibo Yang:** Writing – original draft, Software, Formal analysis, Data curation. **Pingbao Yin:** Writing – review & editing, Supervision, Funding acquisition.

Declaration of competing interest

The authors declare the following financial interests/personal relationships which may be considered as potential competing interests: Wei He reports financial support was provided by National Natural Science Foundation of China. Pingbao Yin reports financial support was provided by National Natural Science Foundation of China. Kaibo Yang reports financial support was provided by Hunan Provincial Innovation Foundation for Postgraduate. If there are other authors, they declare that they have no known competing financial interests or personal relationships that could have appeared to influence the work reported in this paper.

Acknowledgments

The authors gratefully acknowledge the financial support of grants from the National Natural Science Foundation of China (No. 51478051, 52178311). Hunan Provincial Innovation Foundation for Postgraduate, China (CX20220876).

Data availability

Data will be made available on request.

References

Anura3D-MPM-Research-Community, 2022. Anura3D MPM software - scientific manual. Anura3D MPM Research Community.

Bardenhagen, S., 2001. An improved contact algorithm for the material point method and application to stress propagation in granular material. Comput. Model. Eng Sci 2 (4), 509.

Brzeziński, K., Michalowski, R.L., 2021. Diffused arching in embankments supported by non-compliant columns with capping beams. Comput. Geotech. 132, 104031.

BS8006, 2010. Code of practice for strengthened/reinforced soils and other fills: BS 8006-1: 2010. BSi.

Carlsson, B., 1987. Almerad jord–berakning sprinciper for-bankar papalar. Distr. SGI, Linkoping.

Ceccato, F., Beuth, L., Simonini, P., 2017. Adhesive contact algorithm for MPM and its application to the simulation of cone penetration in clay. Procedia Eng. 175, 182–188.

Ceccato, F., et al., 2015. Study of Large Deformation Geomechanical Problems with the Material Point Method. Università degli studi di Padova.

Chen, Y., Cao, W., Chen, R., 2008. An experimental investigation of soil arching within basal reinforced and unreinforced piled embankments. Geotext. Geomembranes 26 (2), 164–174.

Chen, R., Xu, Z., Chen, Y., Ling, D., Zhu, B., 2010. Field tests on pile-supported embankments over soft ground. J. Geotech. Geoenvironmental Eng. 136 (6), 777–785.
CUR226, 2010. Ontwerprichtlijn paalmatrassystemen Design Guideline Piled Embankments. Stichting CUR, Gouda, ISBN: 978-90-376-0518-1, (in Dutch).
EBGEO, 2012. Recommendations for Design and Analysis of Earth Structures Using Geosynthetic Reinforcements-EBGEO. John Wiley & Sons.
Fei, K., Liu, H.-L., 2009. Field test study and numerical analysis of a geogrid-reinforced and pile-supported embankment. Rock Soil Mech. 30 (4), 1004–1012.
Fern, E.J., Soga, K., 2016. The role of constitutive models in MPM simulations of granular column collapses. Acta Geotech. 11 (3), 659–678.
Han, J., Oztoprak, S., Parsons, R.L., Huang, J., 2007. Numerical analysis of foundation columns to support widening of embankments. Comput. Geotech. 34 (6), 435–448.
He, W., Sivakumar, S., Sugawara, J., 2023. Assessment of soft clay characteristic after 40 years of treatment using preloading with wick drains. In: Proc.605 of the 14th Australian and New Zealand Conference on Geomechanics. Cairns 2023 (ANZ2023).
Hewlett, W., Randolph, M., 1988. Analysis of piled embankments. Int. J. Rock Mech. Min. Sci. Geomech. Abstracts 25 (6), 297–298.
Horgan, G., Sarsby, R., 2002. The arching effect of soils over voids and piles incorporating geosynthetic reinforcement. In: Proc., 7th Int. Conf. on Geosynthetics. Balkema Rotterdam, Netherlands, pp. 373–378.
JTG-T-D31-02-2013, 2013. Technical Guidelines for Design and Construction of Highway Embankment on Soft Ground: JTG/T D31-02-2013. China Communications Press Co. Ltd.
King, L., Bouazza, A., Dubsky, S., Rowe, R.K., Gniel, J., Bui, H.H., 2019a. Kinematics of soil arching in piled embankments. Géotechnique 69 (11), 941–958.
King, L., Bouazza, A., Maksimenko, A., Gates, W.P., Dubsky, S., 2019b. Measurement of three-dimensional displacement field in piled embankments using synchrotron X-ray tomography. Can. Geotech. J. 56 (6), 885–892.
King, D., Gniel, J., King, L., Bouazza, A., 2020. Geosynthetic reinforced column supported embankments-designing for serviceability. Aust. Geomech. 55 (1), 27–40.
Lai, H.J., Zheng, J.J., Zhang, R.J., Cui, M.J., 2018. Classification and characteristics of soil arching structures in pile-supported embankments. Comput. Geotech. 98, 153–171.
McGuire, M.P., 2011. Critical Height and Surface Deformation of Column-Supported Embankments (Ph.D. thesis). Virginia Tech.
Naughton, P., 2007. The significance of critical height in the design of piled embankments. In: Soil Improvement. pp. 1–10.
Pan, G., Liu, X., Yuan, S., Wang, Y., Sun, D., Feng, Y., Jiang, G., 2022. A field study on the arching behavior of a geogrid-reinforced floating pile-supported embankment. Transp. Geotech. 37, 100795.
Pham, T.A., Dias, D., 2021. 3D numerical study of the performance of geosynthetic-reinforced and pile-supported embankments. Soils Found. 61 (5), 1319–1342.
Rogbeck, Y., Alén, C., Franzén, G., Kjeld, A., Odén, K., Rathmayer, H., Watn, A., Øiseth, E., 2003. Nordic guidelines for reinforced soils and fills. Nordic Geosynthetic Group of the Nordic Geotechnical Societies, Nordic Industrial Fund.
Rui, R., van Tol, F., Xia, X.L., van Eekelen, S., Hu, G., Xia, Y.-y., 2016. Evolution of soil arching; 2D DEM simulations. Comput. Geotech. 73, 199–209.
Rui, R., Ye, Y.-q., Han, J., Zhai, Y.-x., Wan, Y., Chen, C., Zhang, L., 2022. Two-dimensional soil arching evolution in geosynthetic-reinforced pile-supported embankments over voids. Geotext. Geomembranes 50 (1), 82–98.
Simon, B., 2013. Recommendations for the Design, Construction and Control of Rigid Inclusion Ground Improvement. Presses des Ponts, Paris.
Smith, E.J., Bouazza, A., King, L.E., 2022a. Numerical simulation of the progressive development of soil arching in column-supported embankments. Can. Geotech. J. 59 (2), 159–176.
Smith, E.J., Bouazza, A., King, L.E., Rowe, R.K., 2022b. New insights into soil arching behaviour in column-supported embankments. Can. Geotech. J. 59 (6), 901–921.
Sulsky, D., Zhou, S.-J., Schreyer, H.L., 1995. Application of a particle-in-cell method to solid mechanics. Comput. Phys. Comm. 87 (1–2), 236–252.
Terzaghi, K., 1943. Theoretical soil mechanics.
Van Langen, H., Vermeer, P., 1991. Interface elements for singular plasticity points. Int. J. Numer. Anal. Methods Geomech. 15 (5), 301–315.
Więckowski, Z., 2004. The material point method in large strain engineering problems. Comput. Methods Appl. Mech. Engrg. 193 (39–41), 4417–4438.
Wijerathna, M., Liyanapathirana, D., 2020. Load transfer mechanism in geosynthetic reinforced column-supported embankments. Geosynth. Int. 27 (3), 236–248.
Xu, Z.Z., Chen, R.P., Chen, Y.M., 2008. Field test on technique of cap-pile supported embankment. J. Zhejiang Univ. Science 42, 1484–1488.
Xu, Z.Z., Chen, R.-P., Chen, Y.M., 2009. Study of in-situ data of pile-supported embankment with pile partially penetrated in soft soils. Chin. J. Rock Mech. Eng. 28 (11), 2336–2341.
Yang, G.Q., Wang, X., Wang, X.Z., Jin, J.Z., Zhang, C., 2022. Field tests on mechanical behavior of pile-supported embankment in soft soil area. Chin. J. Geotech. Eng. 44 (11), 2089–2096.
Ye, X., Wu, J.T., Li, G.W., 2021. Time-dependent field performance of PHC pile-cap-beam-supported embankment over soft marine clay. Transp. Geotech. 26, 100435.
Yu, Y., Bathurst, R.J., Damians, I.P., 2016. Modified unit cell approach for modelling geosynthetic-reinforced column-supported embankments. Geotext. Geomembranes 44 (3), 332–343.
Zhang, Q.Q., Li, Z.B., Ma, B., Li, L.L., Li, S.A., Wu, J.Q., 2021. Vertical bearing behavior of rigid and flexible piles in pile-supported embankment. Chin. J. Geotech. Eng. 43 (6), 991–999.
Zhang, L., Luo, Q., Liu, X.X., et al., 2010. Cushion effect analysis of pile-net composite foundation based on field tests. J. Southwest Jiaotong Univ. 45 (5), 787–793.
Zhang, C., Su, L., Jiang, G., 2022. Full-scale model tests of load transfer in geogrid-reinforced and floating pile-supported embankments. Geotext. Geomembranes 50 (5), 896–909.
Zuo, D.J., Qi, C.G., Zhang, Y.T., Liu, x.Q., 2013. Field tests on plastic tube cast-in-place concrete piles for reinforcing soft ground of highways. Chin. J. Geotech. Eng. 35 (9), 1746–1752.